Novel Phase and CFO Estimation DSP for Photonics-Based Sub-Thz Communication

Hae Young Rha, Sang-Rok Moon, *Member, IEEE*, Joon Ki Lee, and Seung-Hyun Cho

***Abstract*—Sub-terahertz (THz)-band communication system has drawn much attention as a promising technology to provide future-proof high data rate services. In a photonics-based sub-THz communication system, the generation of THz wave using free running lasers enables us to make a simple, cost effective and frequency tunable implementation. On the other hand, commercially available lasers have relatively broader linewidth and a large carrier frequency offset (CFO). To mitigate the performance degradations due to phase noise and CFO, a carrier recovery digital signal processing (DSP) algorithm is studied for a sub-THz transmission system. We propose a novel phase estimation algorithm to avoid cyclic slips while minimizing phase estimation error to improve BER performance. Our proposed phase recovery DSP algorithm is demonstrated in a 16-quadrature amplitude modulation (QAM) in a 0.3 THz band photonics-based transmission system. Experimental results show that the measured BER are improved from 8.8×10^{-3} to 3.6×10^{-3} in a 120 Gb/s 16-QAM transmission using the proposed algorithm. A wide range of CFO estimation is also supported for a sub-THz wireless transmission system using off-the-shelf lasers. Recovery of a CFO between −5 GHz and 5 GHz was also successfully demonstrated.**

***Index Terms*—Carrier frequency offset, cyclic slip, phase estimation, photonic technology, sub-THz communication.**

I. Introduction

THE data rate of wireless communication has been increased to meet the ever-increasing demand for data traffic. Due to the nature of the higher carrier frequency, sub-terahertz (THz) wireless communication can provide wider bandwidth services than legacy communications. Thus, sub-THz-band communication has become a promising candidate and has been widely researched for the next-generation wireless communications [1]–[5].

To generate a sub-THz-band signal, electronics- and photonics-based approaches have been used. In a photonics-based approach, optical heterodyne mixing method with two free-running lasers can be used to generate a sub-THz-band signal [4]. A photonics-based sub-THz system using two free-running lasers enables us to make a seamless integration with optical fiber networks and a simple, cost effective, frequency tunable implementation [5]. However, a phase noise and a wide range of carrier frequency offset (CFO) are the major impairments in a photonics-based sub-THz system using free running lasers [5]. A broad linewidth due to free running lasers causes a serious phase noise effect. Moreover, a wide range of sub-THz frequency offset is generated due to the frequency drifts of two free running lasers. To mitigate these effects, optical filtering of optical frequency comb generator was proposed, but it significantly increased the complexity of the transmitter [5].

Phase noise degrades signal power due to spreading, degrades coherence of the demodulation process and adds additive white Gaussian noise (AWGN)-like noise [6]. Since these impacts degrade the performance of communication systems, phase noise mitigation using digital signal processing (DSP) has been researched [7]–[11]. By estimating and compensating for the phase rotation due to phase noise, overall system performance can be improved. In [7], a non-data aided m-th power Viterbi & Viterbi(V&V) algorithm was proposed for phase shift key (PSK) modulations, which uses a block-wise operation to decrease estimation error. Though the m-th V&V algorithm was simple and effective, it could not be directly applied to M-quadrature amplitude modulation (QAM), so the blind phase search (BPS) algorithm was proposed for M-QAM modulation [8]. Since BPS examines the phase estimation through distances between various test phases and received symbols, extensive calculation is required. To decrease the complexity, the maximum likelihood (ML) algorithm or the phase-locked loop (PLL) combined with BPS were proposed [9], [10]. However, these blind algorithms were vulnerable to the cyclic slip problem which comes from 4-fold phase estimation. To solve this cyclic phase slip, a differential coding and decoding could be used. Since differential coding can cause a sensitivity penalty, training assistant phase estimation was proposed [11], which uses the phase difference between regularly inserted pilot symbols and received symbols. However, the insertion of pilot symbols reduces the net data rate and more pilot symbols are required in a system under severe phase noise. Moreover, the linear fitting of phases may not estimate the phase rotation accurately.

In addition to phase noise, carrier recovery DSP for photonics-based sub-THz systems should have an ability to recover a wide range of CFO. Because commercially available lasers have frequency stability within ±2.5 GHz [12], a CFO with a range from -5 GHz to 5 GHz can occur in a practical system based

Manuscript received October 21, 2021; revised December 8, 2021 and January 4, 2022; accepted January 7, 2022. Date of publication January 13, 2022; date of current version May 2, 2022. This work was supported by the Electronics and Telecommunications Research Institute (ETRI) grant funded by the Korean Government under Grant 21ZH1100, Study on 3D Communication Technology for Hyper-Connectivity. *(Corresponding author: Hae Young Rha.)*

The authors are with the Optical Communication Research Section, Electronics and Telecommunications Research Institute, Daejeon 34129, Korea (e-mail: hyrha@miroandi.com; srmoon@etri.re.kr; juneki@etri.re.kr; shc@etri.re.kr).

Color versions of one or more figures in this article are available at https://doi.org/10.1109/JLT.2022.3142347.

Digital Object Identifier 10.1109/JLT.2022.3142347

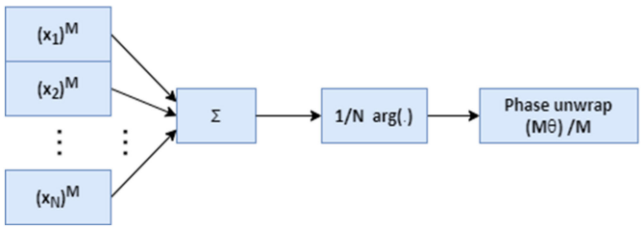

Fig. 1. Block diagram of blind phase estimation using M-th V&V algorithm.

on optical heterodyne mixing technique. Blind phase estimation can be used to recover CFO induced phase rotation. However, it is difficult for a blind phase estimator in an M-QAM system to recover a wide range of CFO. Thus, CFO estimation using a predefined preamble can be adopted to estimate CFO accurately for a wide range [13].

In this paper, a phase estimation DSP algorithm invulnerable to a cyclic slip is investigated to eventually improve BER performance. The probability of cyclic slip depending on various impairments is numerically analyzed and a novel phase estimation is introduced. Finally, a CFO estimation using a preamble is applied to provide a wide and accurate CFO estimation.

II. Phase Estimation Algorithm

A. Blind Phase Estimation and Block Size Optimization

The structure of blind phase estimation using the M-th Viterbi & Viterbi algorithm [7] is shown in Fig. 1. Firstly, the M-th power of symbols removes the data dependent phase due to the modulation format. A block of consecutive *N* symbols is used to estimate the phase and then the block-wise average is applied to mitigate the phase estimation error due to noise such as additive white Gaussian noise (AWGN). The averaged estimated phase is described as follows [14].

$$\theta_n \cong \arg\left\{\frac{1}{N}\left(\sum_{n}^{n+N}\exp\left[iM\varphi\left(k\right)\right]+\sum_{n}^{n+N}q\left(k\right)\right)\right\} \quad (1)$$

where θ is the estimated phase after averaging, φ is the difference between phases of the signal and local oscillator (LO) and $q(k)$ is the k-th phase due to the nonlinear combination of noise and signal. Then phase θ is unwrapped to unfold the M-fold phase.

Block size N is an important factor which affects the performance of a block-wise phase estimator. The phase estimation error due to AWGN can be described using Cramér-Rao bound as the following (2) [8].

$$MSE=\frac{1}{N+1}\left(\frac{E_s}{N_o}\right)^{-1} \quad (2)$$

where *MSE* is the mean square error of phase estimation, and *Es*/*No* is the variance of AWGN. Under the AWGN condition, the estimation error decreases as the block size increases due to the noise cancellation effect.

In the presence of phase noise, however, the optimum block size can exist [8] since the averaging effect of phase noise is not the same as that of AWGN. As the block size increases, phase differences in a block can be increased, which leads to a phase estimation error in a large block.

Moreover, the residual carrier frequency offset (RCFO) can impact the phase estimation performance and optimum block size. Typically, the carrier frequency offset (CFO) is estimated and recovered before phase estimation, but the RCFO can exist due to CFO estimation error. Although phase deviation due to RCFO is symmetric, its affect is not cancelled out because the average in (1) is not applied to the phase but to the complex signal [14]. As the block size increases, phase deviation due to RCFO increases and the effect on the phase estimation error increases as well.

Due to the nature of blind phase estimation in an *M*-fold modulation system, *M* phases in [-π, π) are degenerated into [-π/*M*, π/*M*) and causes *M*-fold ambiguity. Thus, if a phase difference between two consecutive estimations is outside of [-π/*M*, π/*M*), then it leads to a cyclic phase slip. Since a cyclic slip, a permanent integer multiple of a 2π/*M* shift, can cause a long burst of errors, a cyclic slip should be avoided. Even if the mean square error (MSE) of phase estimation is small, one cyclic slip can cause a very high BER due to burst errors. In order to minimize the BER degradation due to phase noise, not only the mean square error of phase estimation but also the cyclic slip probability should be minimized.

In the presence of laser phase noise, the probability of a cyclic slip is expressed as the following (3) [15]. Laser phase noise is modelled as a Wiener process. That means a phase difference between two consecutive phases is modeled as a random Gaussian distributed process with zero mean and a variance $\sigma^2=2\pi\beta T$, where β is the linewidth of laser and T is a symbol period.

$$CS=2Q\left(\frac{\pi}{4\sigma}\right)=2Q\left(\frac{\pi}{4\sqrt{2\beta T}}\right) \quad (3)$$

where Q is the Q-function defined as

$$Q\left(x\right)=\frac{1}{\sqrt{2\pi}}\int_{x}^{\infty}\exp\left(-j\frac{z^2}{2}\right)dz \quad (4)$$

In addition to intrinsic phase noise due to oscillators, a phase estimation error due to AWGN and an RCFO can affect the probability of a cyclic slip. In the next section, the impact of impairments on the cyclic slip probability is numerically obtained.

B. Impact of Impairment on the Probability of Cyclic Slip

The impacts of AWGN, phase noise, and a CFO on the probability of a cyclic slip were simulated in a 16-QAM transmission with the Baud rate of 30 GS/s as shown in Fig. 2. The linewidth of the modulation laser, phase noise1, was set to 100 kHz and the linewidth of local oscillator (LO), phase noise 2, was set to 100 kHz, 1 MHz, and 10 MHz. In the simulation, the blind phase search (BPS) [8] was used as a phase estimation algorithm and cyclic slip probability as a function of block size of the phase estimator was obtained. Simulation results are shown in Fig. 3, where the total number of symbols per point is around 8.4×10^8.

Fig. 3(a) shows the impact of phase noise and AWGN on the cyclic slip probability. As expected, the probability of a cyclic

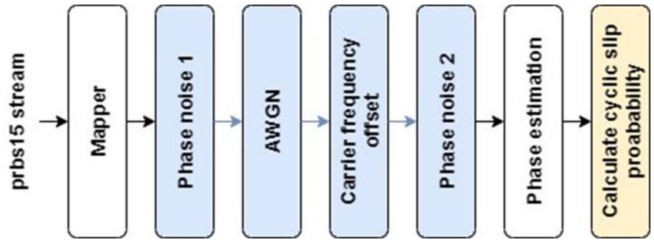

Fig. 2. Block diagram of cyclic slip probability simulation.

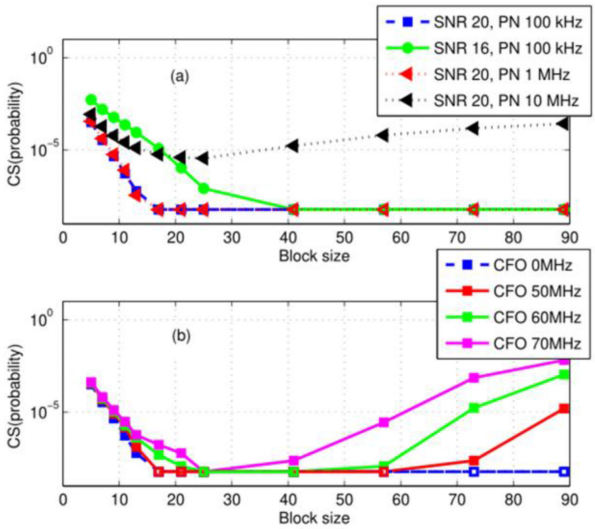

Fig. 3. Cyclic slip probability as a function of block size in the presence of (a) AWGN, laser phase noise (b) AWGN with SNR of 20 dB, laser linewidth of 100kHz and CFO in a 16-QAM system; unfilled symbols: no cyclic slip found.

slip decreases as the block size increases in the presence of AWGN due to the noise cancellation effect. When the block size is small, symbols in a block are not spread to all 4-fold constellation points which increase the phase estimation error in a BPS and the probability of a cyclic slip as well. In case of lower SNR, the probability of a cyclic slip and the minimum block size to avoid a cyclic slip increases. This was also expected because phase estimation error increases in a lower SNR as shown in (2) and thus the probability of cyclic slip coming from estimation error increases.

Cyclic slip probabilities with a linewidth of 100 kHz and 1 MHz did not show much difference at 20 dB SNR. However, for severe phase noise, i.e., a linewidth of 10 MHz, the probability of cyclic slip was bigger than 10^{-6} in any block size. In this case, cyclic slip can be avoided by using a data-aided phase estimation algorithm [11].

Fig. 3(b) shows the cyclic slip probability as a function of block size depending on the presence of a CFO. A CFO of 60 MHz, the normalized CFO to the 30Gbaud rate of 2×10^{-3}, seriously affected the probability of a cyclic slip in higher block sizes. Since the average of estimated phase errors in a block is applied to complex signal, the effect of phase deviation is not fully cancelled out [14]. Phase deviation due to CFO rather was accumulated in larger block sizes, which degraded estimation

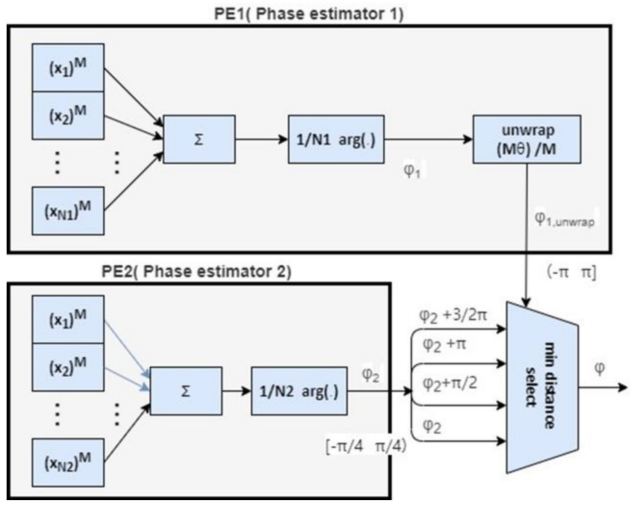

Fig. 4. Block diagram of the proposed phase estimation algorithm.

performance and the probability of cyclic slip was increased as a block size increased.

Thus, the residual CFO(RCFO) after the CFO recovery should be reduced to prevent burst errors induced by a cyclic slip. Since the RCFO depends on the accuracy of CFO estimation, the accuracy of CFO estimation should be considered in a sub-THz communication system based on photonics. As an example, the accuracy of CFO estimation based on auto–correlation depends on the sample interval [16]. In the presence of AWGN, as the sample interval increases, the accuracy of the CFO estimation increases. By increasing the sample interval, the probability of cyclic slip coming from the residual CFOs can be decreased.

C. Our Proposed Carrier Phase Estimation

To obtain high-performance phase estimator, the algorithm consists of two phase-estimation procedures and a minimum phase distance selector is proposed as shown in Fig. 4. The two phase estimation procedures were designed to minimize a cyclic slip and mean phase estimation error. In the following, M-th power Viterbi & Viterbi algorithms are used to explain the proposed algorithm, however, specific block phase estimation algorithms depend on the system specification such as a modulation format or a modulation level. For example, in a 16-QAM transmission system, BPS can be used as a phase estimation algorithm. In the following example, a 4-fold system such as QPSK, is assumed, i.e., M is 4, and non-data aided phase estimator is used.

The first phase estimator 1(PE1) is employed to prevent a cyclic slip and has the estimation range of $[-\pi\ \pi)$. $N1$, the block size of PE1, is chosen to minimize the probability of cyclic slip. The purpose of the second phase estimator (PE2) is to track the phase rotation caused by phase noise and residual CFO and thus minimize the mean phase estimation error. The block size of PE2, $N2$, is chosen to minimize the phase estimation error in the range of $[-\pi/4\ \pi/4)$.

To prevent cyclic slip while minimizing phase estimation error, two estimated phases are combined as follows. The

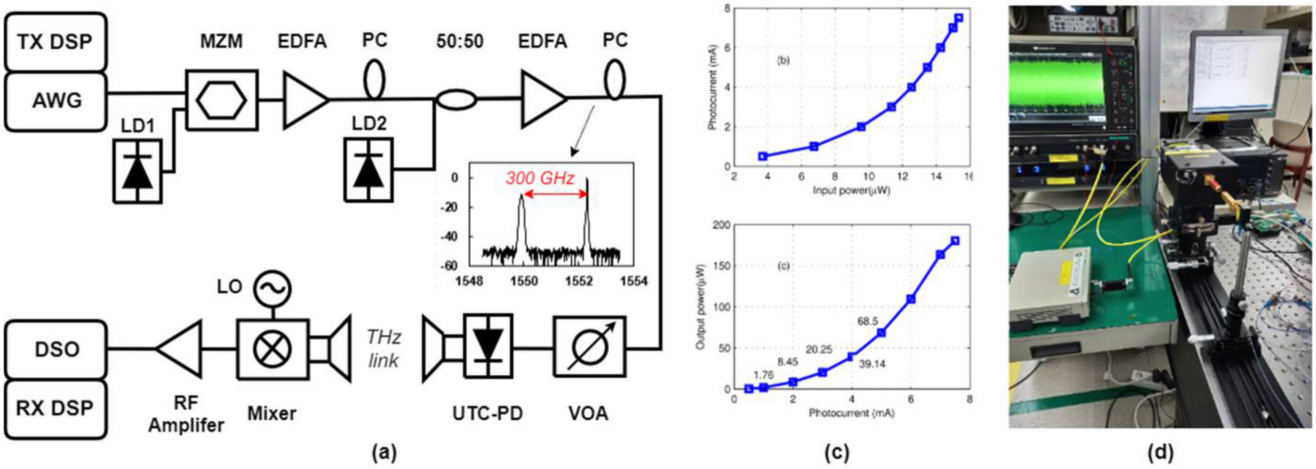

Fig. 5. (a) Experimental setup of sub-THz transmission; LD: laser diode; MZM: Mach-Zehnder modulator; EDFA: Erbium-doped fiber amplifier; PC: polarization controller; VOA: Variable optical attenuator; OSA: optical spectrum analyzer; UTC-PD: uni-travelling carrier photodiode, DSO: digital sampling oscilloscope, LO: local oscillator, (b) photocurrent of the UTC-PD as a function of input power (c) output power of the UTC-PD as a function of photocurrent at a carrier frequency of 300 GHz, (d) photo of the actual setup.

estimated phase φ_1 is unwrapped to obtain unfolded phase $\varphi_{1,unwrap}$ in the PE1 and the estimated phase in the second estimator , φ_2 , is unfolded as φ_2, $\varphi_2 + 2\pi/M$, …, and $\varphi_2 + 2\pi * (M-1)/M$. An estimated phase is finally selected among unfolded phases by searching for the phase with minimal distance as follows.

$$\varphi(n) = \varphi_2(n) + \frac{2\pi}{M}\hat{m} \tag{5}$$

$$\hat{m} = \underset{m}{\operatorname{argmin}} \left(abs \left(\varphi_2(n) + \frac{2\pi m}{M} - \varphi_{1,unwrap}(n) \right) \right),$$

where n is a symbol index, m is 0, 1, ⋯, M-1, and *abs*(.) is an absolute value. Second phase estimation has a lower estimation error but 4-fold ambiguity and is vulnerable to a cyclic slip. By choosing the one among 4 unfolded phases of φ_2, with the minimal distance from $\varphi_{1,unwrap}$, the final phase estimation is decided. Thus, the estimation error of the final phase estimation depends on the second phase estimator PE2 and the probability of cyclic slip of the final estimation depends on the first phase estimator PE1.

III. Experimental Setup and Result

A. Experimental Setup

To evaluate the proposed phase estimation algorithm in a photonics-based sub-THz wireless transmission system with free running lasers, our experiment was carried as shown in Fig. 5(a). Fig. 5(b) and (c) depict the photocurrent of the UTC-PD as a function of optical input power and the output power of the UTC-PD as a function of photocurrent at 300 GHz. The photograph of the actual setup is shown in the Fig. 5(d). A 16-QAM modulated baseband signal was generated in an arbitrary waveform generator (AWG) with pseudo-random bit sequence (PRBS) 2^{15} -1 sequence. In order to generate the sub-THz signal using optical heterodyne mixing, two free running continuous-wave (CW) lasers were employed. Laser diode 1 (LD1) was an external cavity laser (ECL) with a linewidth of 100 kHz. A directly modulated distributed feedback (DFB) laser with a linewidth of 1 MHz or a ECL with linewidth of 100 kHz were used as LD2 to compare the phase noise effect on the BER performances. An electrically modulated baseband signal generated in the AWG was externally modulated at the Mach-Zehnder modulator (MZM) and one output light from LD1 was launched into the MZM. The wavelength difference between LD1 and LD2 was set to 300 GHz. The combined light was amplified by an erbium-doped fiber amplifier (EDFA), and then a variable optical attenuator (VOA) was employed to control the input power of the optical signal into a uni-travelling carrier photodiode (UTC-PD). Then the sub-THz wave was generated at the UTC-PD.

A sub-THz-band signal at the UTC-PD was emitted with horn antennas with a 26 dBi gain to compensate for free space path loss and emitted. Experiments were carried in an optical back-to-back condition.

At the wireless receiver, the beam was down-converted to the intermediate frequency (IF) domain using a THz mixer (VDI SAX 3.4) with a bandwidth of 40 GHz and a conversion loss of 14 dB. Then, the IF band signal was amplified using an RF amplifier with bandwidth of 40 GHz. Then the IF band signal was captured by a real-time digital sampling oscilloscope (DSO) with a 36 GHz bandwidth and 80 GS/s sampling rate. The sampled digital signal was processed with the receiver DSP at a personal computer.

Fig. 6 shows the frame format and the structures of the transmitter and the receiver DSP. A frame started with a preamble, which was inserted to provide a wide and accurate CFO estimation [13] and the length of preambles was 576 with a sample interval of 288. After a preamble was attached, 3840 training symbols were attached to train a channel equalizer in the receiver DSP and followed by a data sequence with a length of 34560 symbols.

At the transmitter, a bit sequence was firstly mapped to the gray mapped 16-QAM signal. After a preamble was inserted, signal was oversampled, and a square raised cosine (SRRC)

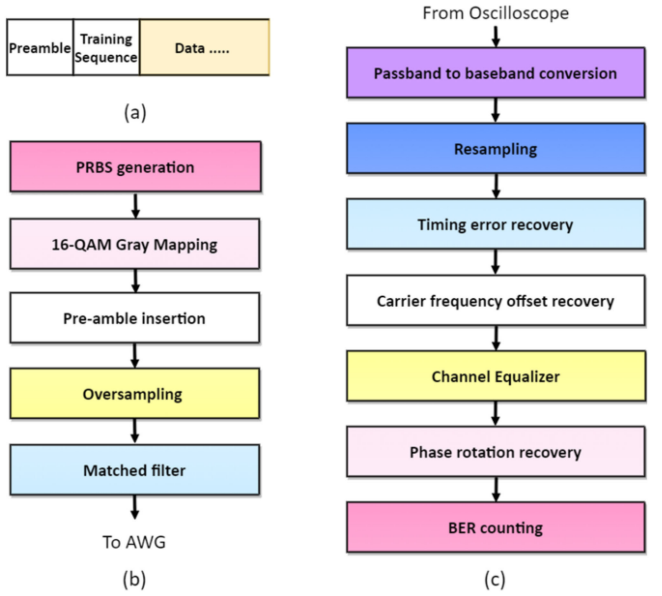

Fig. 6. (a) Frame format, (b) transmitter, and (c) receiver DSP structures for sub-THz transmission.

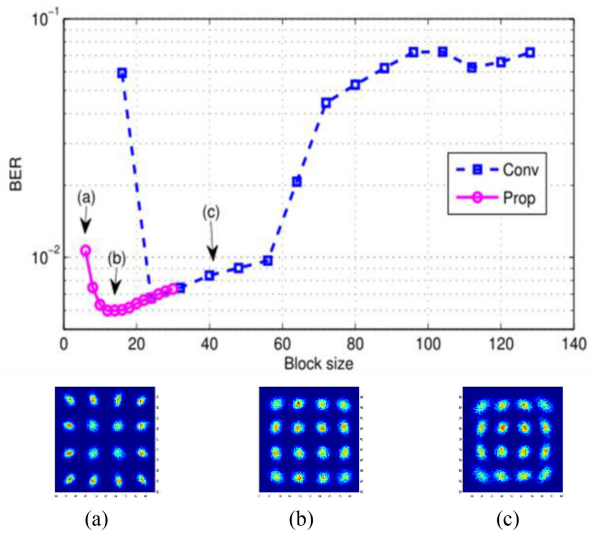

Fig. 7. BER as a function of block size in a 16-QAM 30 GBaud transmission with 100kHz LD1 and 1MHz LD2. Constellations of the block size of (a) 2 (b) 14, and (c) 40.

filter with a roll-off factor of 0.4 was applied to two-oversampled signal. Then the two-oversampled samples were resampled at a rate of AWG of 100 GS/s.

At the receiver DSP, the received signal was captured by the digital oscilloscope at a rate of 80 GS/s. The received signal in the passband was post-emphasized [1] and converted into a baseband signal. A low pass filtered baseband signal was resampled at the rate of two times of baud rate. Then, the timing error recovery system estimated and compensated for the initial timing offset by finding the value to minimize the metric using a square time algorithm [17] to track the sampling phase offset quickly. Then a timing error recovery with a feedback structure was used, which consisted of an interpolator for a timing recovery, a phase detector with a square time algorithm [17] and a second order loop filter. After timing error recovery, a preamble for CFO estimation was searched by finding the time index to maximize auto-correlation between the timing recovered signals. The CFO recovered signal was post-equalized with the pre-measured equalized filter coefficients then fed into a radius directional equalizer (RDE) which consisted of a T/2-spaced 31-tap feed forward equalizer (FFE). Phase rotation was estimated from the equalized signal using the BPS [8], a data-aided phase detection [11] and our proposed phase estimation algorithm. Then a phase recovered signal was de-mapped into a bit stream. A BER counter was connected at the output of the de-mapper to calculate an uncoded BER.

B. Experimental Results of Phase Estimation

Firstly, the block size needed to be determined for conventional and our proposed phase estimators. Optimum block sizes depend on the phase noise condition. As an example, block sizes were obtained in 30 GBaud transmission with LD1 had a 100 kHz linewidth and the LD2 had a 1 MHz linewidth as follows. Received samples in the digital oscilloscope were saved and the block size was swept for the stored signals to obtain optimum block sizes as shown in Fig. 7. A BPS [8] was used as a non-data aided phase estimator and the number of test phases for the BPS was set to 32.

For the conventional phase estimator, the block size can be chosen from the BER curve shown in Fig. 7. In smaller block sizes, AWGN noise and phase noise generated a number of cyclic slips. As a block size increased, phase estimation errors were increased and BERs were degraded. In a block size larger than 60, there was an abrupt BER degradation due to cyclic slip. From Fig. 7, the block size can be set to 40, a middle point between 25 and 56 which didn't generate cyclic slip, to minimize the probability of cyclic slip.

For the proposed algorithm, two block sizes need to be decided. The block size, *N1* can be selected to prevent a cyclic slip and the block size chosen for a conventional algorithm, 40, can be used. Once block size *N1* was decided, the block size *N2* was swept. From Fig. 7, the block size *N2* can be set to 14 to obtain the optimum BER performance.

For the small *N2*, two, the constellation was squeezed as shown in Fig. 7(a), and the BER was high. This was because two symbols in a block were rotated to have minimal distance from the constellation points with the large phase estimation error due to the small noise cancellation effect of block-wise average. At the block size of *N1*, 40, Fig. 7(c) shows the drifting constellations and it seems that phase estimator couldn't track the phase rotation quickly due to the large block size. Thus, the overall BER performance was maximally improved when the block size to minimize the cyclic slip possibility is used as *N1*, and the *N2* block size of 14 to have fast tracking ability is used as shown in Fig. 7(b), where the constellations were shaped as circles.

Fig. 8 shows the measured BERs as a function of the photocurrent in the UTC-PD. Fig. 8(a) shows the measured BERs of 30 GBaud transmission using two ECLs with a linewidth of 100 kHz

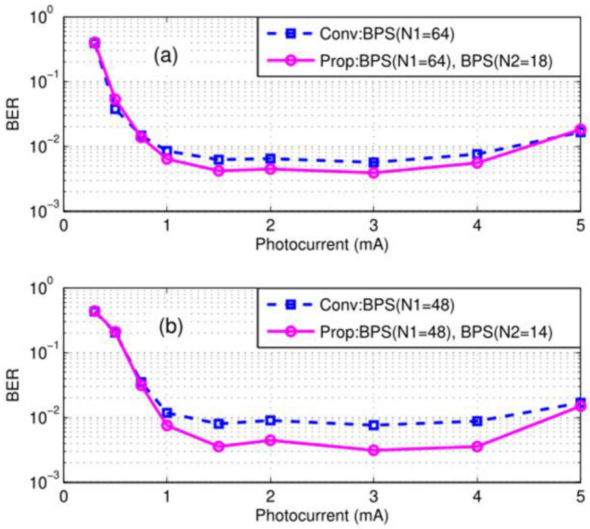

Fig. 8. Measured BER as a function of UTC-PD power; blue line: conventional method (BPS) and the proposed algorithm with two BPSs. (a) 100 kHz LD2. (b) 1 MHz LD2.

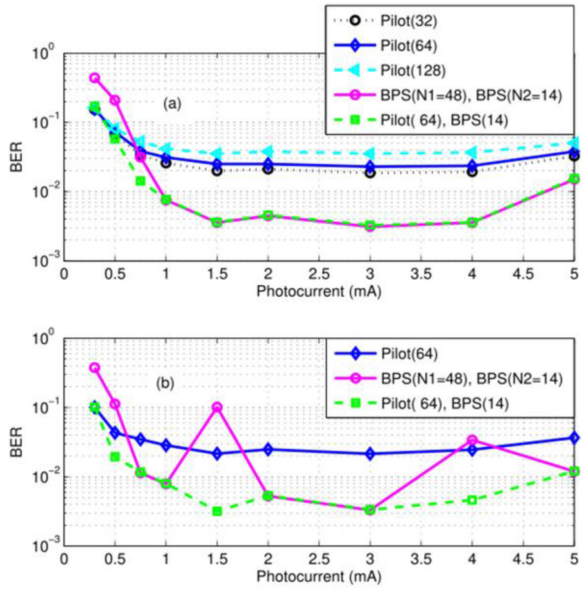

Fig. 9. Measured BER as a function of UTC-PD power for the conventional method using pilot symbol, the algorithm using pilot symbol and a BPS [18], and the proposed algorithm with two BPSs in (a) 30 GBaud, (b) 20 GBaud transmission.

where the block size N1 and N2 were optimally chosen as previously described and were set to 64 and 18, respectively. In this case, BER performance were slightly improved from 5.6×10^{-3} to 3.9×10^{-3} at the photocurrent of 3 mA. Fig. 8(b) shows the measured BERs for a 30 GBaud transmission when the LD1 had a 100 kHz linewidth and the LD2 had a 1 MHz linewidth. At a photocurrent of 4 mA, the BER improved from 8.8×10^{-3} to 3.6×10^{-3}. The performance improvement of the latter case was higher than that of the former case. More severe phase noise seems to be the reason of higher BER improvement of the latter. In the wireless sub-THz transmission, the performance of phase estimation was improved by applying the proposed algorithm and thus BER as well. We think that the proposed algorithm could be applied to estimate phase in any optical system.

C. Phase Estimation Using a Pilot Symbol

In a severe phase noise condition, a training-assisted phase estimation algorithm would be used as a first phase estimator (PE1) as an alternative of the proposed algorithm. Using regularly inserted pilot symbols, phase differences between transmitted symbols and received symbols can be obtained [11]. Fig. 9 shows the measured BER as a function of photocurrent for a conventional data-aided algorithm with different pilot symbol intervals, of 32, 64, and 128, the algorithm with a data-aided algorithm using a pilot symbol to prevent cyclic slips and a blind estimator [18] and the proposed algorithm with two blind phase estimators. BERs of 30 GBaud and 20 GBaud with two LDs with a linewidth of 100 kHz and 1 MHz are shown in Fig. 9(a) and (b), respectively. For the conventional algorithm, as the pilot symbol interval was increased the BER was degraded.

In the 30 GBaud transmissions with the photocurrent larger than 0.75mA, the BER of the proposed algorithm with two BPSs was the same with that of the algorithm using a pilot symbol [18]. This was expected because the accuracy of the phase estimation was decided by the second phase estimator. In the low photocurrent conditions, it seems that cyclic slips were generated for the proposed algorithm with two BPSs due to the low SNR.

In the 20 GBaud transmission, however, the BER of the proposed algorithm with two BPSs showed unstable BER performances and cyclic slip caused high BER at the photocurrent of 1.5mA and 4mA. In the 20 GBaud transmission, we failed to find a block size of a blind estimator which did not generate any cyclic slip at the wide range of UTC-PD photocurrent. It seems that the higher phase noise condition coming from the lower baud rate of 20GBaud than 30GBaud caused the cyclic slips. In this severe phase noise condition, pilot symbols can be used to prevent cyclic slips and Fig. 9(b) shows the stable performance of the algorithm with data-aided estimator and a blind estimator. Despite of the overhead of pilot symbols, a data-aided phase estimator can be used to avoid a cyclic slip in a severe phase noise condition because a data-aided phase estimator removes a 4-fold ambiguity of a blind phase estimator in the 16-QAM constellation.

D. Experimental Result of CFO Recovery

Carrier phase recovery system should support a wide range of CFO estimation in a practical photonics-based sub-THz wireless transmission system. The CFO estimator using a predefined preamble [13] can be adopted to estimate a large CFO accurately. To demonstrate the CFO recovery range, the frequency of the local oscillator (LO) was swept from -5 GHz to 5 GHz as shown in Fig. 10. In Fig. 10, BERs were slightly degraded as the CFO increases and it seems that narrow bandwidth of the system caused BER degradations for large CFOs.

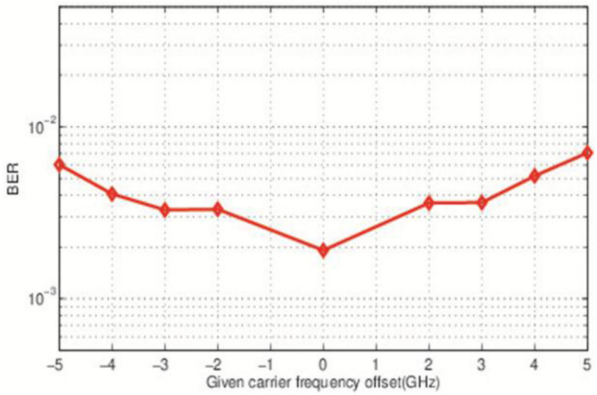

Fig. 10. Measured BER as a function of the given CFO.

IV. Conclusion

Sub-THz communication is a promising technology for the next generation wireless communication. However, a photonics-based sub-THz communication system suffer from severe phase noise and a large carrier frequency offset (CFO), especially when two free-running LDs are used for cost effectiveness. To analyze performance degradation due to a cyclic slip, we numerically analyzed the probability of a cyclic slip depending on various impairments such as SNR, phase noise and residual carrier frequency offset (RCFO). Simulation results showed that the accuracy of CFO is needed to be considered to reduce the probability of a cyclic slip. To improve the BER performance of a sub-THz communication system, we proposed a novel phase estimation algorithm, which combines two phase estimation procedures to prevent cyclic slips and minimize phase estimation error. We experimentally demonstrated the proposed phase estimation algorithm in the 0.3 THz wireless transmission system using two free running lasers. The BER was improved from 8.8×10^{-3} to 3.6×10^{-3} in the 30 GBaud 16-QAM transmission. Moreover, we successfully demonstrated a wide range of CFO recovery between -5GHz and 5GHz. In conclusion, a simple, cost-effective sub-THz wireless transmission system using free running lasers becomes more feasible using our proposed phase estimation and CFO estimation DSP.

References

[1] S. Jia *et al.*, "0.4 THz photonic-wireless link with 106 Gb/s single channel bitrate," *J. Lightw. Technol.*, vol. 36, no. 2, pp. 610–616, Jan. 2018.
[2] T. Nagatsuma and G. Carpintero, "Recent progress and future prospect of photonics-enabled terahertz communications research," *IEICE Trans. Electron.*, vol. 98, no. 12, pp. 1060–1070, 2015.
[3] T. Harter *et al.*, "Generalized Kramers–Kronig receiver for coherent terahertz communications," *Nature Photon.*, vol. 14, no. 10, pp. 601–606, 2020.
[4] S. Moon *et al.*, "6G indoor network enabled by photonics- and electronics- based sub-THz technology," *J. Lightw. Technol.*, early access, 20 Sep. 2021, doi: 10.1109/JLT.2021.3113898.
[5] L. Gonzalez-Guerrero *et al.*, "Single sideband signals for phase noise mitigation in wireless THz-over-fibre systems," *J. Lightw. Technol.*, vol. 36, no. 19, pp. 4527–4534, Oct. 2018.
[6] R. P. Gilmore, "Specifying local oscillator phase noise performance: How good is good enough?," in *Proc. IEEE Int. Symp. Pers., Indoor Mobile Radio Commun.*, 1991, pp. 166–172.
[7] A. Viterbi, "Nonlinear estimation of PSK-modulated carrier phase with application to burst digital transmission," *IEEE Trans. Inf. Theory*, vol. 29, no. 4, pp. 543–551, Jul. 1983.
[8] S. H. T. Pfau and R. Noe, "Hardware-efficient coherent digital receiver concept with feed-forward carrier recovery for M-QAM constellations," *J. Lightw. Technol.*, vol. 27, no. 8, pp. 989–999, Apr. 2009.
[9] X. Zhou, "An improved feed-forward carrier recovery algorithm for coherent receivers with M-QAM modulation format," *IEEE Photon. Technol. Lett.*, vol. 22, no. 14, pp. 1051–1053, Jul. 2010.
[10] X. Zhou and Y. Sun, "Low-complexity, blind phase recovery for coherent receivers using QAM modulation," in *Proc. Opt. Fiber Commun. Conf.*, 2011, Paper OMJ3.
[11] X. Zhou and L. Nelson, "Advanced DSP for 400 Gb/s and beyond optical networks," *J. Lightw. Technol.*, vol. 32, no. 16, pp. 2716–2725, Aug. 2014.
[12] Integrable Tunable Transmitter Assembly Multi Source Agreement OIF-ITTA-MSA-01.0, 2008.
[13] H. Y. Rha, C. J. Youn, E. S. Nam, and H.-W. Choi, "Simple full-range carrier frequency offset estimation for high speed CO-OFDM," *Opt. Exp.*, vol. 21, no. 20, pp. 23896–23906, 2013.
[14] E. Ibragimov, B. Zhang, T. Schmidt, C. Malouin, N. Fediakine, and H. Jiang, "Cycle slip probability in 100G PM-QPSK systems," in *Proc. Opt. Fiber Commun. Conf.*, 2010, Paper OWE2.
[15] S. T. Le, P. A. Haigh, A. D. Ellis, and S. K. Turitsyn, "Blind phase noise estimation for CO-OFDM transmissions," *J. Lightw. Technol.*, vol. 34, no. 2, pp. 745–753, Jan. 2015.
[16] T. M. Schmidl and D. C. Cox, "Robust frequency and timing synchronization for OFDM," *IEEE Trans. Commun.*, vol. 45, no. 12, pp. 1613–1621, Dec. 1997.
[17] M. Oerder and H. Meyr, "Digital filter and square timing recovery," *IEEE Trans. Commun.*, vol. 36, no. 5, pp. 605–612, May 1988.
[18] M. A. Castrillon, D. A. Morero, and M. R. Hueda, "A new cycle slip compensation technique for ultra high speed coherent optical communications," in *Proc. IEEE Photon. Conf.*, 2012, pp. 175–176.

Hae Young Rha received the B.S. degree in physics from Korea University, Seoul, South Korea, in 1994, the M.S. degree in physics from Seoul national University, Seoul, South Korea, in 1996, and the Ph.D. degree from the Electronic Engineering Department, Korea Advanced Institute of Science and Technology, Daejeon, South Korea, in 2015. From 1996 to 2009, she was a Semiconductor Logic Designer with Hynix, Samsung Electronics and Electronics and Telecommunication Research Institute. Since 2015, she has been a Principal Engineer with Miro&I Co. Her research interests include the design and implementation of high-speed optical communication DSP.

Sang-Rok Moon (Member, IEEE) received the B.S. degree in physics , and the M.S. and Ph.D. degrees in electrical engineering from the Korea Advanced Institute of Science and Technology, Daejeon, South Korea, in 2008, 2010, and 2015, respectively. Since 2015, he has been with the Electronics and Telecommunication Research Institute, Daejeon, South Korea, where he is currently a Senior Researcher. His current research interests include high-speed optical transmission systems, digital signal processing in optical networks, and photonics-based THz-band communication systems.

Joon Ki Lee received the M.S. degree in applied physics from the Gwangju Institute of Science and Technology, Gwangju, South Korea, in 1997, and the Ph.D. degree in electronics engineering from Chungnam National University, Daejeon, South Korea, in 2016. From 1997 to 2001, he was an Engineer with Hanwha Information and Telecommunications Corporation. Since 2001, he has been with Electronics and Telecommunications Research Institute, Daejeon, South Korea, where he is currently the Managing Director of Optical Networking Research Section. His research interests include high-speed optical transmission systems, optical transceivers, data center network, and optical-mobile converged access network.

Seung-Hyun Cho received the B.S. and M.S. degrees in electronic materials engineering from Kwangwoon University, Seoul, South Korea, in 1997 and 1999, respectively, and the Ph.D. degree in materials science and engineering from Hanyang University, Seoul, South Korea, in 2010. From 1999 to 2000, he was with the Access Network Laboratory of Korea Telecom, Daejeon, South Korea. Since 2000, he has been with the Electronics and Telecommunication Research Institute, Daejeon, South Korea, where he is currently a Project Leader for THz short-distance transmission technology based on photonics. His current research interests include next-generation optical access network, mobile fronthaul and DAS for 5G networks, and THz wireless delivery system. He is also the Chair of IEC TC103 (transmitting equipment for radiocommunication) and Co-Editor of G.9803 (radio over fiber systems) in ITU-T SG15/Q2.